Automatic Core Logging using Core Imagery and Deep Learning

by

Shirley Shuocheng Zhang

An undergraduate thesis
presented to the University of Toronto
for the degree of
Bachelor of Applied Science
in
Civil Engineering

Toronto, Ontario, Canada, 2022

Author's Declaration

I hereby declare that I am the sole author of this thesis. This is a true copy of the thesis, including any required final revisions, as accepted by my advisor.

I understand that my thesis may be made electronically available to the public.

Abstract

Recent advancement in Machine Learning (ML) has demonstrated promising results in a variety of applications due to its powerful ability to identify patterns in data and make predictions. In particular, ML is increasingly being applied in the mining exploration industry to perform drill-core logging based on geophysical data, geochemical data, RGB imagery, and hyperspectural imagery. This thesis summarizes the current state of the field which reveals several potential research directions. A list of existing commercial products in development is also included.

As a proof of concept, a 2D semantic segmentation model is developed using U-Net to calculate RQD in core samples. The prediction by the ML model is compared to human-labeled data to determine the prediction accuracy. In addition, a web-based platform is implemented to provide an interactive and easy-to-use interface for the ML workflow and to dynamically display the results. Finally, conclusions and recommendations are made based on any important findings. A summary of publicly available databases is attached at the end for future development.

Acknowledgements

I owe my deepest gratitude to my thesis advisor, Dr. Sebastian Goodfellow, who has always been approachable and supportive throughout my final year of study. His encouragement and understanding created opportunities for me to develop research ideas and helped me overcome challenges. I am also grateful to Kore Geosystems for sharing their software which has been tremendously helpful. This project would not have been possible without the data the generally provided. Finally, I would like to thank the faculty and staff in the Civil and Mineral Engineering department at the University of Toronto for their assistance and help throughout my undergraduate study.

Table of Contents

List of Figures

List of Tables

Chapter 1

Introduction

1.1 Problem Description

Drill-cores are cylindrical rock samples that are extracted from the ground for the exploration of sub-surface mineral resources. Core characteristics such as rock type, texture, alteration facies, ore-forming minerals, and structures provide valuable geological information on potential ore accumulations [8]. However, logging cores by visual inspection is a time-consuming task, and the consistency of results depends on the experience of individual geologists. As a result, other analytical techniques such as optical microscopy, X-ray diffraction (XRD), X-ray Fluorescence (XRF), scanning electron microscopy (SEM), and Laser Ablation Inductively Coupled Plasma Mass Spectrometry (LA-ICP-MS) are performed on selected samples to provide mineralogical and geochemical information [9]. Hyperspectral (HS) imaging is another emerging technique that is capable of performing mineral mapping (i.e., determining the spatial distribution of minerals) in a large number of drill-cores in a fast and noninvasive manner [10].

With drastic advances in computational power and an increasing availability of large datasets, the traditionally knowledge-driven mineral exploration industry is pivoting toward a more data-driven approach capable of leveraging machine learning techniques. A traditional machine learning model makes predictions based on the relationships and patterns it learned from example data. For example, a machine learning algorithm can be trained to predict rock names based on the geochemical composition of the rock (Figure 1.1). During training, it is given examples of geochemical compositions with the associated labels (i.e., rock names) and learns the relationship between them. Using this estimated relationship, the model will approximate the underlying function in the data and attempt to predict rock names given different compositions.

Whereas traditional machine learning algorithms are suitable for processing structured data that can easily be stored in a relational database (i.e. assay data), deep learning

(DL) algorithms such as convolutional neural networks (CNN) are suitable for processing complex, unstructured data such as images. A CNN model learns patterns in the data progressively, from simple relationships between variables in the first layers to complex abstract patterns in the last layers (Figure 1.2). Another popular DL model is the recurrent neural network (RNN), which specializes in processing temporally connected data presented as sequences of inputs such as time series. For example, RNN can be used to log borehole data based on continuous rock physical properties measurements.

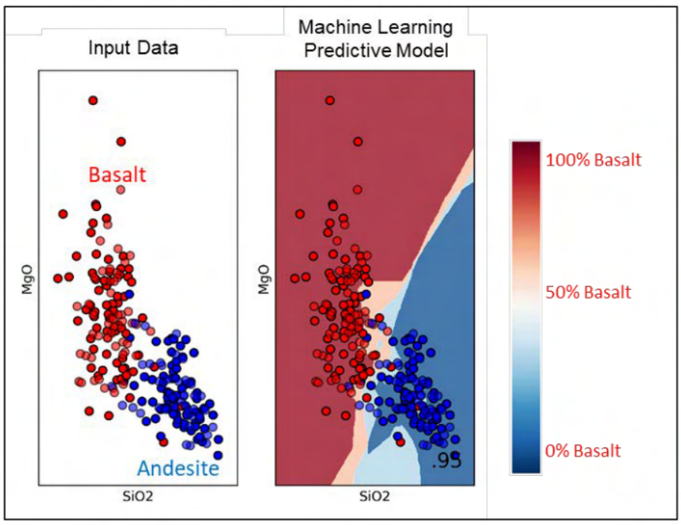

Figure 1.1 A traditional machine learning model that predicts rock names based on their geochemical composition [1].

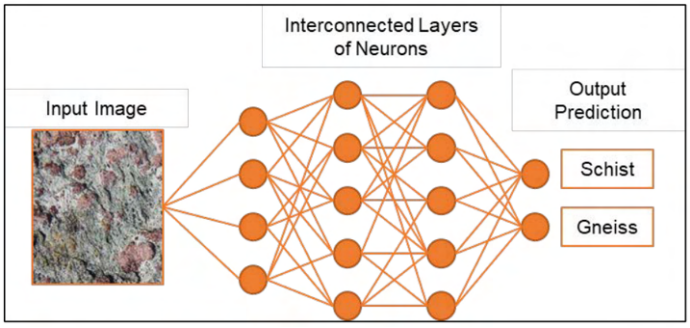

Figure 1.2 A Deep Neural Network that predicts rock names from photographs [1].

1.2 Literature Review

A wide range of data can be obtained from the drill-cores to extract valuable information from a (potential) mineral deposit. This review will focus on the application of ML on geophysical data, geochemical data, RGB image, and hyperspectral image to support core logging processes.

1.2.1 Geophysical Data

To compensate for the increasing difficulty of deposit discovery, new geophysical data-collection tools with downhole sensors are introduced to the mining industry and provides rock physical properties as standard data available during drilling campaigns [2]. To cope with the enormous amount of data acquired at an almost continuous rate (Figure 1.3), recently-developed machine learning techniques can be applied to make predictions and aid in the decision making process. Combined with machine learning algorithms, these large multivariate data sets can help geologists predict information such as mineralization and facies from geophysical logs. Some example applications of geophysical data are illustrated below.

1.2.1.1 Resources estimation

Contrary to base metals, the presence of gold mineralization in drill core is difficult to assess even for an experienced geologist. One study detected gold-bearing intervals from geophysical logs by integrating ensemble machine learning algorithms (random forest (RF) and gradient tree boosting) with rock physical properties measured at closely spaced intervals along the drill core [2]. Supervised learning was selected for this application because both the desired output signals (a binary classification of samples having a gold value higher or lower than a threshold) and the predictive variables (logs and derived statistics) were known in the training samples. Since the prediction was continuous along the drill core, this model could help geologists decide which intervals to select for assay sampling. It also has the potential to increase the reserve by reduce the amount of missed gold-bearing intervals.

1.2.1.2 Facies Prediction

A similar workflow used to predict the presence of certain minerals in drill core can also be applied to predict geological facies (i.e., bodies of rock with specified characteristics) [11]. In this study, a random forest classifier was trained to classify five geological facies highlighting rock types and alteration assemblages with a sixth facies to assess the case of

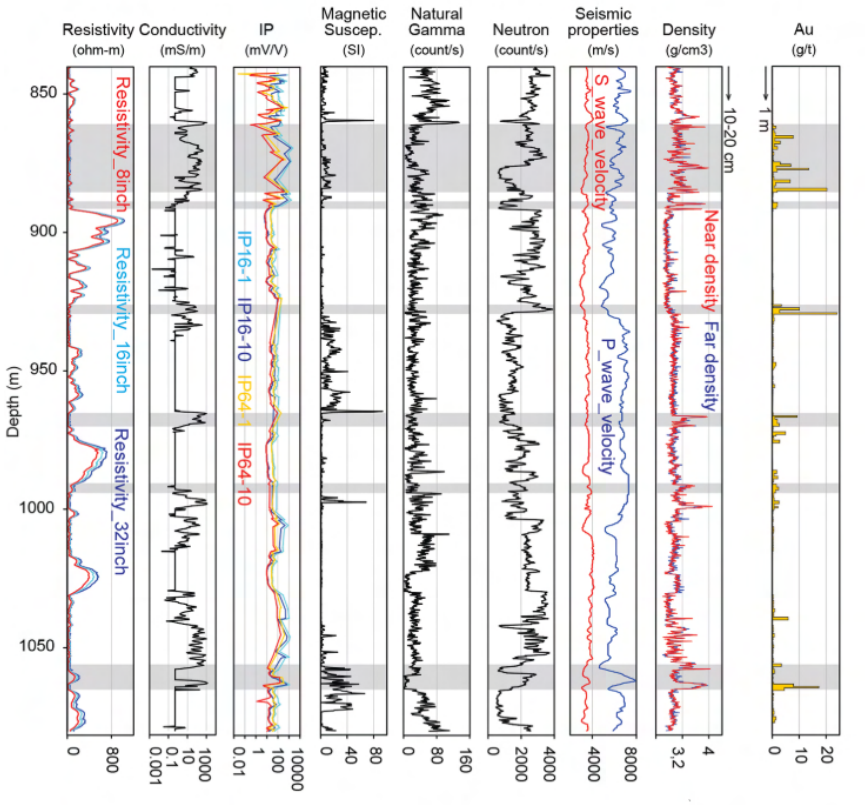

Figure 1.3 Combined rock physical properties and metal assay data along a section of a drill hole [2]

drill-hole casing. The overall prediction was generally accurate with the exception of altered zones and sulphides, as alteration mineral assemblages showed progressive transitions and are hard to discriminate even for a trained geologist.

1.2.1.3 Other applications

Along with predicting the presence of metals and facies in rocks, geophysical properties aided by machine learning have the potential to classify lithologies, characterize hydrothermal alteration, and estimate exploration vectors and geotechnical information in the drill-core [12]. A combination of these predictions will significantly improve the quality of core-logging and geologic interpretations during a drilling campaign or during mine exploitation [11].

1.2.2 Geochemical Data

In addition to supervised machine learning algorithms, unsupervised machine learning techniques such as self-organizing maps (SOM) can be applied to geochemical datasets to automate aspects of drill-core logging. A study at the George Fisher mine performed SOM analysis on XRF scans from Minalyzer CS and found that it was not only effective in recognizing distinct clusters in the data, which correlated well with the lithology logs from the mine, but was able to introduce a greater variety in rock type recognition [13]. Based on this analysis, a classification scheme was developed to automatically distinguish between different rock types according to varying elemental compositions of the rock, which in turn automated the preliminary geological drill-core logging process. In particular, the XRF analysis recognized the specific quantity of elements, e.g. iron content in pyritic shale, which could not be assessed by eye. One limitation is that although the automated logging could pick up small lithological changes from the 10 cm-scale with no extra required time, the logging at mine-scale did not possess the same amount of detail expected from mine geologists due to practical limits.

In another study, a method called Data Mosaic was proposed to incorporate spatial information into geochemistry data to improve rock type classification [14]. Although drill hole data are spatial data (i.e. each measurement is taken at a specific location in space), this spatial information is not usually considered when applying ML to drill hole data due to uncertainties in determining a suitable spatial scale. However, results from ML algorithms applied to drill holed without reference to spatial information typically result in small-scale units at the width of a single sample due to misclassfication. Data Mosaic allowed rock type classification to be applied simultaneously across a range of spatial scales for each drill hole by grouping samples of similar composition into spatially connected domains. The multiscale domains provided a framework for the application of machine learning techniques such as k-means. Data Mosaic was demonstrated using high spatial resolution XRF data from a drill-core, and the ability to apply the method to large data sets was demonstrated using multi-element chemistry data from a densely drilled deposit.

Not only can machine learning be used for classification tasks (e.g., rock type recognition), it can also be used for regression (e.g., prediction a continuous variable such as a geochemical element). One study uses machine learning to estimate a key missing geochemical variable, sodium, from multiparameter data which contains density, magnetic susceptibility, 15 geochemical elements, average visible light reflectance, and infrared spectrometry [15]. Because the correlations between sodium and the other variables were weak, the data did not show Gaussian distributions, and the data were clustered in multiple classes, methods like multiple regression or support vector machine (SVM) were not suitable for this application. Instead, the random forest algorithm was selected based on its simplicity of use as well as its ability to quantitatively rank the most important variables, and the

algorithm achieved a usable estimate of sodium at high spatial resolution. In a different study, the random forest algorithm was applied (along with principal component analysis and discriminant analysis) to lithogeochemistry of sandstones obtained from drill-cores to identify elements associated with uranium [16].

1.2.3 Hyperspectral Image

The mining industry is gradually integrating the use of hyperspectral (HS) sensors, which records hundreds of spectral bands along the electromagnetic spectrum, to complement drill-core analyses. [17]. HS data provides continuous compositional (mineralogy) information along the core face, different spectral filters can be applied to emphasize specific mineralogical properties [6]. Borehole scans also are non-destructive, and the data can be used throughout the project life cycle. In addition, one can make use of complementary information from different imaging sensors (e.g., combining hyperspectral and RGB imagery) to provide important information for resource modelling [18].

Recently, machine learning classification techniques have been suggested for drill-core HS data analysis to improve its robustness and automation. For example, a study used a data fusion approach (i.e., combining high resolution mineralogical data with HS data) to train a supervised classification model [19]. To address the lack of available training samples for the classification, the authors used SEM based mineral liberation analysis (SEM-MLA) to generate training labels for the classification of HS data. Two machine learning algorithms, RF and SVM, were selected for the classification task because they could handle high-dimensional data with a limited number of training samples. A subsequent study also combined the two datatypes and upscaled the quantitative SEM-MLA mineralogical data to drill-core scale to obtain quasi-quantitative maps over entire drill-core samples [20].The procedure wass tested using random forests (RF), SVM and neural network regression models to obtain mineral abundance maps that are used for the extraction of mineralogical parameters such as mineral association.

To improve on the traditional classification methods, a multi-label classification concept was introduced for the mineral mapping task in drill-core hyperspectral data analysis, which had the advantage of considering different mineral mixtures present in each pixel [21]. The drill-core hyperspectral data used in this paper covered the visible-near infrared (VNIR) and the short-wave infrared (SWIR) range of the electromagnetic spectrum. A Classifier Chain method (CC) was implemented using the RF algorithm as the base classifier to provide meaningful and descriptive mineral maps.

Another study integrated hyperspectral and the previously-mentioned geochemical data via a super-pixel-based machine learning framework [9]. The authors extracted labels from the geochemical assays and selected representative samples for each measurement from the hyperspectral data. A supervised machine learning classification (composite kernel Support

Vector Machine) was then used to extrapolate the elements relative abundance to the entire core length. Subsequently, the authors proposed a way to integrate hyperspectral data covering different regions of the electromagnetic spectrum in a kernel-based framework to facilitate the identification of a larger amount of elements. Results demonstrated the super-pixel approach is more accurate than the pixel-based approach and has the potential to reduce geochemical assays needed for the detailed core analysis.

1.2.4 RGB Imagery

Although geochemical analysis, geophysical surveys and multispectral images are viable techniques, geologists still commonly interpret lithologies, alteration types, or exploration vectors from drill-core using visual observations due to the cost and time consumption associated with those quantitative methods [22]. However,there are a number of drawbacks associated with visual geological description:

1. They are subjective and qualitative to at most semi-quantitative;
2. They are not reproducible as results vary between geologists and time periods;
3. Quality assessment and control are difficult to implement on visual descriptions;
4. The data collected is limited, and core boxes need to be unstacked if further information is required.

To correctly detect rock type from a large amount of images in a relatively short amount of time, automated processes are being developed by a number of companies and research groups in the mining industry. In 2017, Mezghani et al. performed automated core sample analysis using high definition core photos taken in daylight [23]. In addition, missing parts of the core (for example, cylindrical samples from full core or "plugs") were reconstructed from fullbore microimager images (FMI) and surrounding structure and texture by multi-point statistic (MPS). The disadvantage of this approach was a reduction in precision, and this work did not compare all images with image samples library to estimate lithology by contrast and pixel intensity.

To speed up the description process and improve the description quality, machine learning tools are increasingly being applied to automatically generate drill-core descriptions that can be used by logging geologists as a basis for their own descriptions. Ivchenko et al. used deep convolutional neural networks to classify six types of rocks from segmented core images taken in daylight and UV light under different conditions (light intensity, angle, resolution etc.) [24]. Another recent study compared the performance of several well-known convolutional neural network architectures (AlexNet, VGG, GoogLeNet, ResNet) on lithology classification [25]. It was concluded that ResNet and VGGNet concentrated on the grain

size of the lithotype, as each filter emphasized the granularity of an image. ResNet did not extract information from images when the size of grains was small. However, VGGNet attempted to extract information in all cases. GoogLeNet activations concentrated more on texture classification. In addition, some limitations to CNN classification were discovered: 1) some lithotypes can produce comparable structures; 2) images may contain two or three lithotypes, which leads to misinterpretation; 3) some lithotypes are incorrectly classified due to fine grain size or similarity of structures.

More information on the automatic analysis of core images can be found in the Commercial Products Section below.

1.3 Commercial Products

With the rise of machine learning in the mining industry, both start-ups and well-established companies are developing products and services for automated core logging. More specifically, a number of companies are focusing on extracting geological and geotechnical information from drill-core imagery. For example, CGG GeoSoftware's Powerlog is a general petrophysical interpretation software that contains a module for supervised and unsupervised facies classification. geoLEARN's Predikor describes lithologies, alteration, and veins along drill-core automatically based on linearized core images. These algorithms learn from already described drill-cores to produce a predictive model for a particular deposit. These descriptions are reproducible and quantitative, and they can be adapted to a project and modified at will by retraining the model.

DiUS and Solve Geosolutions' Datarock Core offers a more comprehensive drill core imagery processing workflow. Using a range of PyTorch-based image analysis techniques such as image classification, object detection, and both semantic and instance segmentation, the application turns raw images into a structured format and segments the important geological information. The Mask R-CNN model, combined with Detectron2 (a PyTorch-based computer vision library), is used to improve segmentation tasks [26]. Some specific features include rotation and distortion corrections, cropping, depth registration, textural domaining, vein segmentation and orientation measurement, fracture detection and orientation measurement, RQD estimation, and custom segmentation models (Figure 1.4) (Figure 1.5).

GoldSpot's LithoLens is another core imaging technology that turns old core images into intact, georeferenced core images and uses deep learning algorithms to enhance the images and extract valuable geological information.This is done by eliminating aspects of the image that are not rock, optimize the quality of the existing image, and automatically recognize varying geological intervals – or specific features such as veins – within the core.

Minalyze's Minalyzer CS is a scanner that generates geochemistry, highresolution im-

Figure 1.4 RQD estimation using CNN [3].

ages, rock quality designation (RQD), structures, specific gravity and bulk density for drill-cores in a contactless way. It is capable of scanning drill-cores directly in core trays, generating a 3D-model of the topology of the core and trays with a laser (LiDAR), and performing continuous XRF scanning. RQD and structures are also derived based on the 3D-model. The continuous nature of the datasets and the compact data density are extremely helpful in machine learning and deep learning applications.

Taking the scanner one step further, KORE Geosystems' SPECTOR is a fully integrated system that combines a core imaging system with a cloud-based AI product that is capable of segmenting rock, classifying lithology and alteration, detecting veins, and localizing fractures. Other applications that utilize machine learning to extract features for geological classification include enthought's Virtual Core and IMAGO's Learn.

In terms of hyperspectral imagery, Life Cycle Geo's Intellicore evaluates hyperspectral image for brownfields exploration by recognizing hyperspectral image intervals representing variable distance to mineralization. The application is also used for operational grade control by identifying hyperspectral imagery representing variable grade ore for block modeling and segregation purposes. Another application of Intellicore is environmental waste management to identify waste materials with variable acid rock drainage and metals leaching potential.

The following steps are taken by Intellicore to prepare and process hyperspectral data using deep learning algorithms:

1. Data analysis: Unsupervised methods (e.g., clustering, principal component analysis)

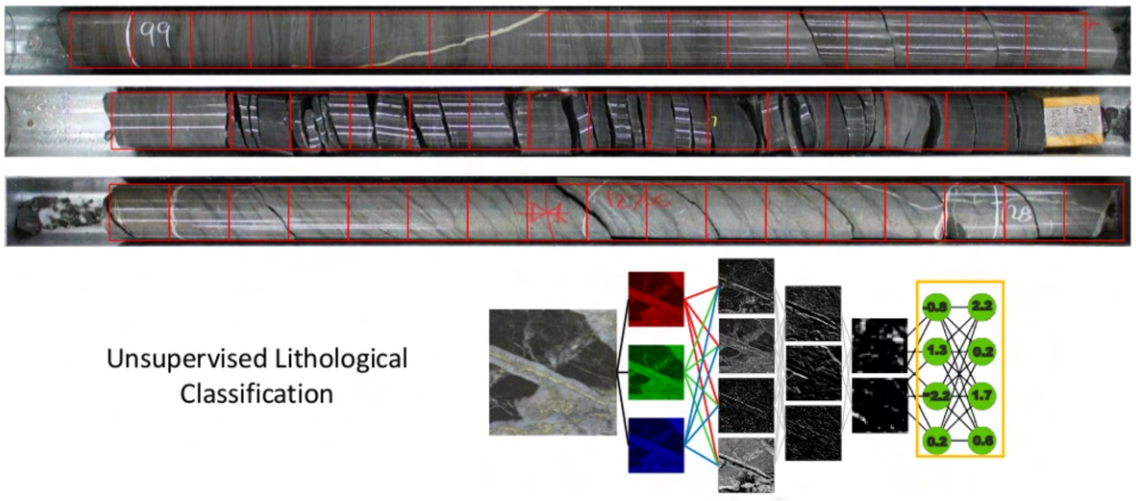

Figure 1.5 Unsupervised lithological classification using CNN [3].

are used to explore quantitative data obtained from hyperspectral imagery, to both understand its structure and reduce its dimensionality. This analysis determines how the hyperspectral imagery is filtered and weighted.

2. Gaps and core loss: Depth tags placed in the core box by the logging geologist are analyzed to address gaps in core and calculate core loss for accurate depth registration.

3. Image concatenation and splitting: Hyperspectral images from different core boxes are joined together to form one long borehole image so that they can then be split into the image length required for deep machine learning. This accounts for the fact that images from different core boxes can be of different resolution (pixel/distance density) and width.

4. Deep learning modeling: Images are ported into a cloud-based, deep learning environment where neural network algorithms can be applied. Model results report a predictive accuracy, which can be improved by iteratively performing the previous steps (especially unsupervised analysis).

Chapter 2

Hypothesis

2.1 Calculating RQD using Semantic Segmentation

As previously described, geologists and engineers perform core logging to extract data from drill cores, which informs many aspects of the mining industry such as exploration, resource estimation, mine design, extraction, processing, remediation. While a wide range of data can be observed from core imagery, in the interest of time, this thesis will focus on Rock Quality Designation (RQD). Proposed by Deere and Deere in 1988 [27], RQD is a measure of quality of rock taken from a borehole, and it is based on the amount of fractures in the rock mass that is observed from the drill cores (Figure 2.1). RQD can be calculated by summing and dividing intact pieces longer than 10 cm by the total length of the drill core [27]:

$$RQD = \frac{\sum(\text{length of core fragments} > 10\text{cm}}{\text{total core length}} \times 100 \tag{2.1}$$

RQD is an important parameter in drill core logging because it informs geotechnical engineering decisions such as foundation depth, bearing capacity, and settlement possibilities [4]. Conventional RQD labelling is performed via visual observation, which is subjective, time-consuming, and non-reproducible. In addition, collecting RQD is a repetitive and difficult process, which naturally lends itself to automation. More specifically, image segmentation methods have the potential to perform rock segmentation by predicting the boundaries of rock fragments and measuring them.

After researching and experimenting with different image segmentation models, U-Net was chosen as the desired method for RQD calculation. U-Net is a symmetrical image segmentation architecture with encoding and decoding modules [5]. The model contains a contracting path that captures context, as well as a symmetric expanding path that enables precise localization (Figure 2.2). Since RQD calculation is a visual measuring task and not a

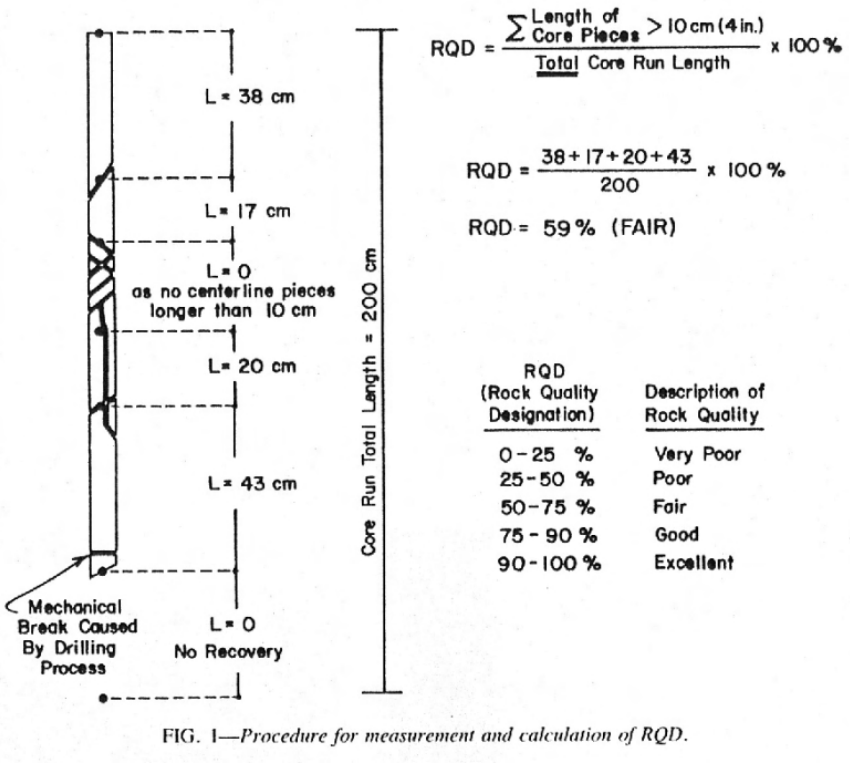

FIG. 1—*Procedure for measurement and calculation of RQD.*

Figure 2.1 RQD Calculation [4].

classification task, being able to assign a class label to each pixel is critical in this application. In addition, while successful training of typical deep networks require many thousands of annotated training samples, U-Net utilizes strong data augmentation strategies to use the available annotated samples more efficiently. As a result, it can be trained end-to-end from very few images while outperforming the prior best method (a sliding-window approach) for segmentation of biomedical images. Because there are very few public datasets containing 2-D labelled core photographs, and annotating training images manually is a very tedious process, the U-Net architecture provides an advantage over traditional CNN methods. In addition, since we are mostly interested in separating core from background pixels and do not care about labelling individual core pieces, semantic segmentation is sufficient for our purpose as opposed to instance segmentation (where each piece would be assigned a different label). A post-processing algorithm can be applied to calculate the lengths of each detached rock. However, if time permits, instance segmentation algorithms such as Mask-RCNN may be explored and compared with the U-Net approach.

This paper aims to develop a semantic segmentation approach to calculate RQD in core samples using U-Net, then deploy the model to a web application. An ML-powered, web-based platform will automate the analysis of drill core imagery and significantly improve

its efficiency. Figure 2.2 is a sample workflow comparison between the traditional core-logging process and the ML alternative. It is worth noting that the application of ML is not meant to replace the geologists but to aid their decision making process for time-saving and error-prevention purposes.

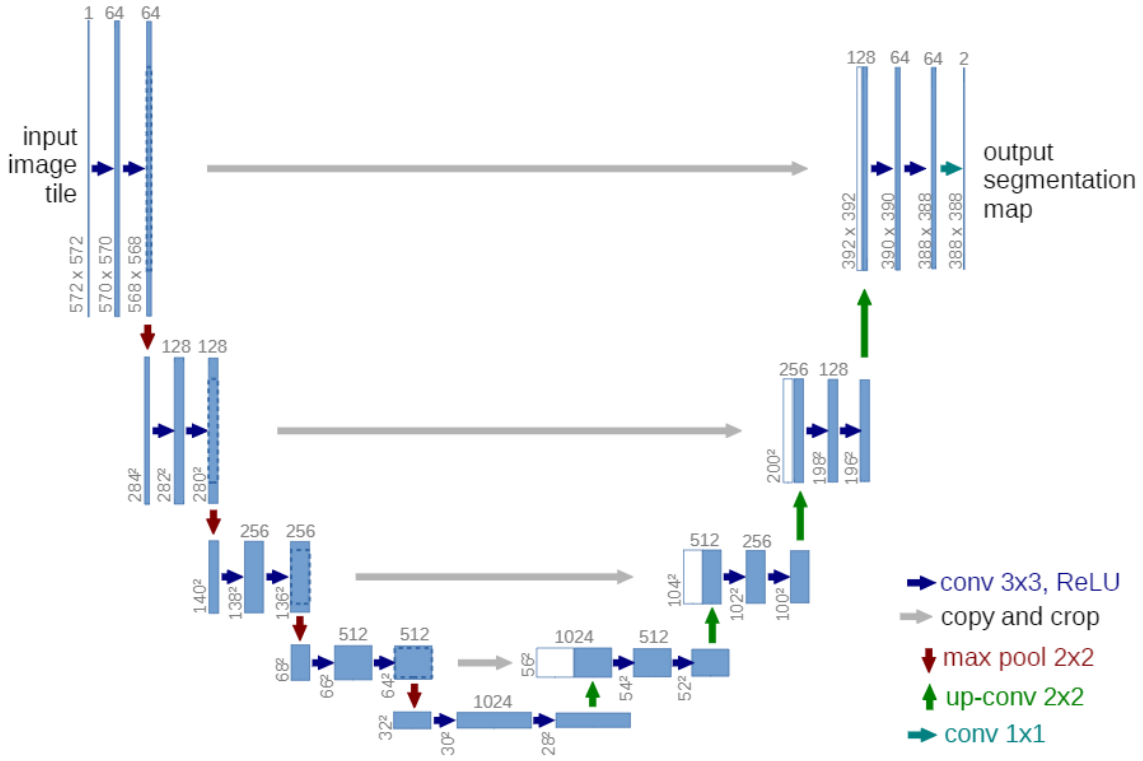

Figure 2.2 U-net architecture [5].

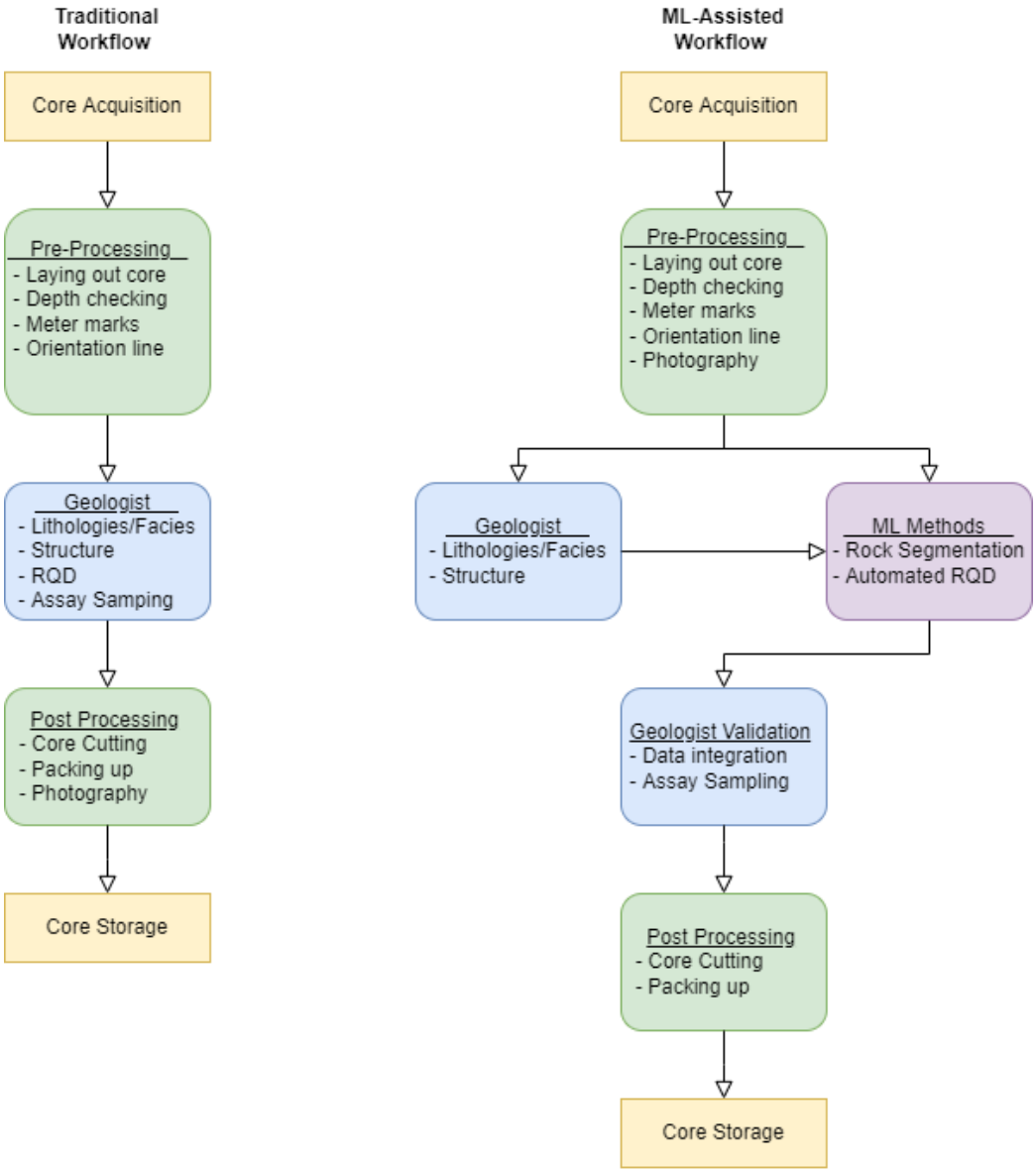

Figure 2.3 Traditional v.s. potential ML-assisted workflow for drill-core description [6].

Chapter 3

Procedure

3.1 Data Acquisition

Like most Machine Learning projects, the first step in the workflow is to obtain reliable datasets of core images with RQD labels. Eight labelled images were found from an online repository of the British Geological Survey [28]. In addition, forty-two core photographs were acquired from Kore Geosystems [29] and labelled manually using the LabelMe tool developed by the Computer Science and Artificial Intelligence Laboratory (CSAIL) at MIT [30]. The result of the labelling process is demonstrated in Figure 3.1.

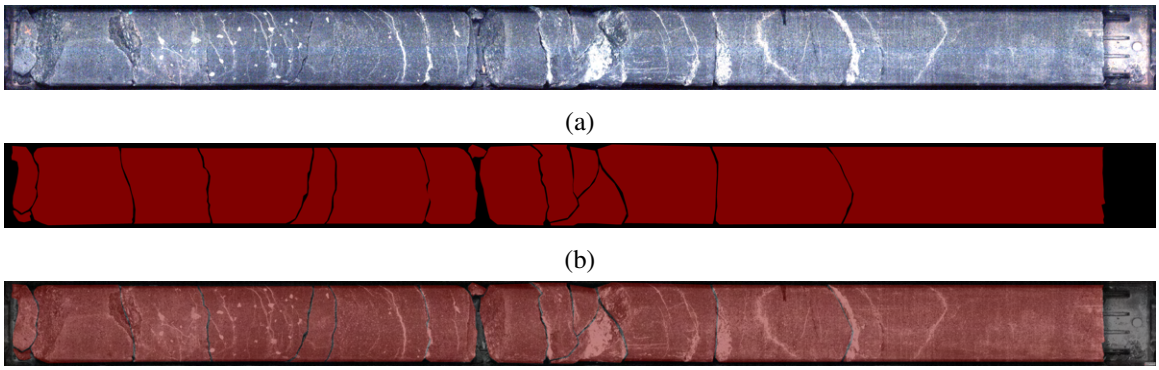

(a)

(b)

(c)

Figure 3.1 (a) Original core photograph (b) Mask created using LabelMe (c) Mask overlaid on top of original image for illustration.

3.2 Data Pre-processing

Following data acquisition and labelling, images are downsized by 6-fold (from 14101x1028 to 1350x170) due to limitations in resources. The downsized images can be trained on

Google Colab Pro which offers an Nvidia P100 or T4 GPU and up to 25GB RAM [31]. An image before and after downsizing is illustrated in Figure 3.2. Although it may be difficult to spot the differences visually from the images, downsizing does affect the image quality especially when it comes to finer cracks.

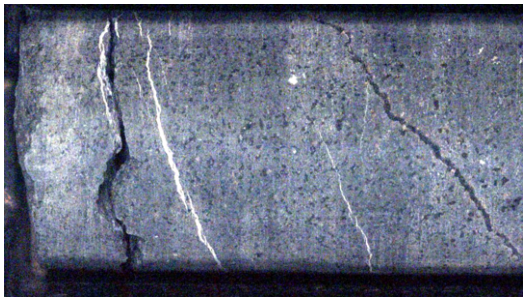

(a) Cropped section of an original image

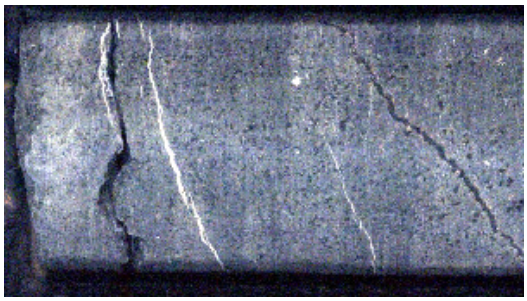

(b) Cropped section of a downsized image

Figure 3.2 Comparison between original image and downsized image

In addition to downsizing, some pre-processing techniques are applied to improve the quality of the labels. For example, an erosion operator can applied to the original mask to further isolate individual elements [32]. Erosion computes a local minimum over the area of given kernel and causes the the brighter areas to get smaller, whereas the dark zones gets bigger. The effect of erosion is illustrated in Figure 3.9.

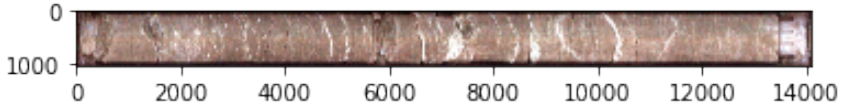

(a) Original image

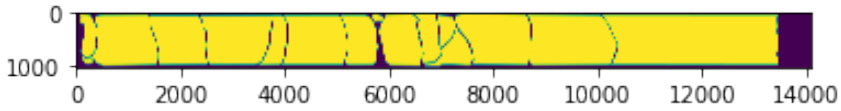

(b) Non-eroded mask

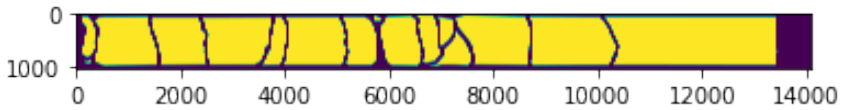

(c) Eroded mask

Figure 3.3 Comparison between eroded and non-eroded mask

The 50 core images are divided into training, validation, and test dataset using a 60/20/20 split. In addition, various data augmentation strategies are applied to the training dataset as a regularization technique. Instead of training the model with the same images, small

transformations are applied to improve generalizability [32]. The transforms used in this project include flipping, rotating, zooming in, change in lighting, and warping as shown in Figure 3.4. Note that no transformation is applied to the validation dataset except for resizing.

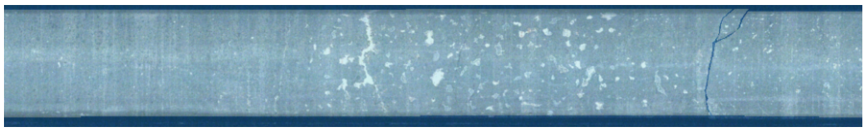

(a) Validation image without transformation

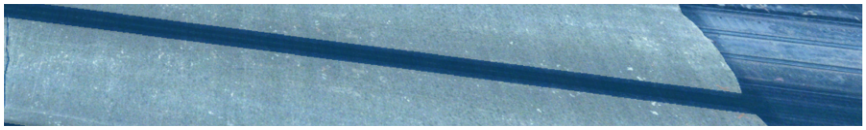

(b) Training image with transformation

Figure 3.4 Effect of transformation

3.3 Image Segmentation

The U-Net model used in this project is built from a ResNet34 backbone pre-trained on ImageNet using transfer learning. ImageNet is a large image dataset with around 14 million images divided into over 100,000 subsets [33]. Making use of a model that has been pre-trained on millions of other images is a common way to improve prediction accuracy. This transfer learning approach is also applied during training time by training the model on smaller sized images at first, then increase the size until we reach the full image.

Resnet is a residual learning framework where the layers are formatted to learn residual functions with reference to the layer inputs instead of learning unreferenced functions [7]. As illustrated in Figure 3.5, residual learning can be realized by the introduction of "skip connections". As a result, these residual networks are easier to optimize and can gain accuracy from substantially increased depth.

Organized experiments are conducted to optimize the U-Net architecture and fine-tune certain parameters to suit our specific task. For example, as shown in Figure 3.6, the optimal learning rate (LR) is found by examining the loss at different learning rates. The accuracy function is a metric for evaluating model performance and updating model weights at each epoch. for segmentation, we want to squeeze all the outputted values to have it as a matrix of digits for our segmentation mask. From there, we want to match their argmax to the target's mask for each pixel and take the average. The resulted accuracy function is shown in Figure 3.7.

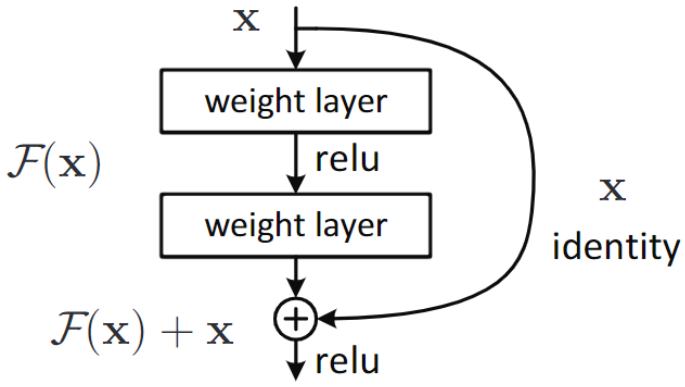

Figure 3.5 Building block in residual learning with skip connection [7].

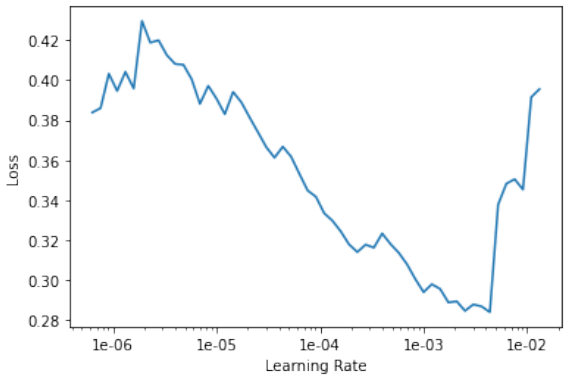

Figure 3.6 Learning rate finder.

Some of the model configurations I focused on tuning are shown below. The model is trained on Google Colab using the Tesla P100-PCIE-16GB GPU and 26.3GB available RAM [31].

1. Blur/blur final: avoid checkerboard artifacts
2. Self attention: A self-attention layer
3. y range: Last activations go through a sigmoid for rescaling
4. Last cross: Cross-connection with the direct model input
5. Bottle: Bottleneck or not on that cross
6. Activation function: e.g., ReLU, Mish
7. Norm type

```
target = target.squeeze(1)
mask = target != LABELS.index("Void")
return (input.argmax(dim=1)[mask]==target[mask]).float().mean()
```

Figure 3.7 Loss function for image segmentation.

3.4 Data Post-Processing

After the initial prediction, post-processing algorithms can be used to refine the quality of predicted masks. For example, a dilation operator and an erosion operator can be applied sequentially to the predicted mask to smooth out any edges. Figure 3.8b shows the resulted prediction when only erosion is applied. Figure 3.8c shows the resulted prediction when both dilation and erosion are applied. It is evident that dilation is useful in filling in any unintentional gaps that would otherwise be enlarged by erosion. However, dilation should be applied carefully to avoid joining two separate pieces together as seen on the left side of Figure 3.8c.

(a) Original predicted mask

(b) Eroded mask

(c) Dilated and eroded mask

Figure 3.8 Effect of dilation and erosion on predicted mask

It is also important to pay attention to the number of iterations an operator is being applied. As shown in Figure 3.9, without enough iterations, the pieces won't be separated effectively. On the other hand, too much erosion may lead to the loss of smaller pieces.

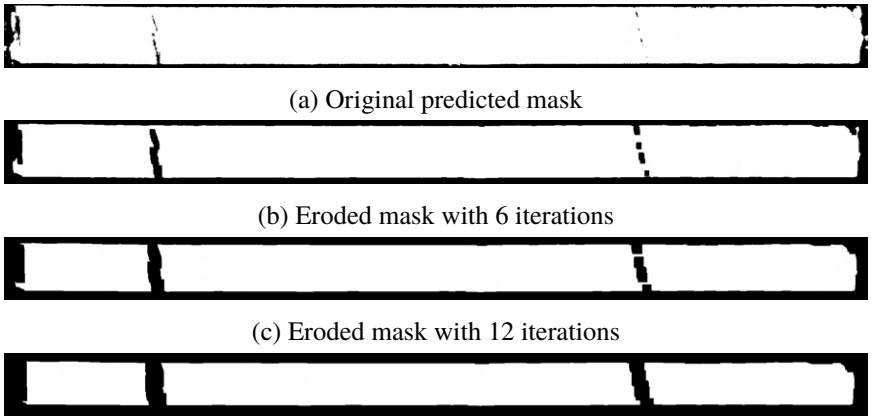

(a) Original predicted mask

(b) Eroded mask with 6 iterations

(c) Eroded mask with 12 iterations

(d) Eroded mask with 18 iterations

Figure 3.9 Effect of the number of iterations on erosion

3.5 RQD Estimation

Finally, after post-processing, RQD can be estimated based on the area of each detached rock fragment. As shown in Figure 3.10, Image Processing modules from OpenCV are used to find and draw contours on the predicted masks [32]. The watershed algorithm is also applied to extract touching or overlapping pieces [32].

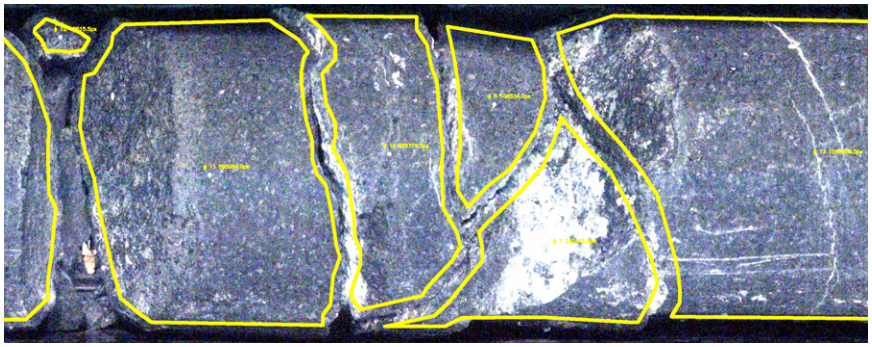

Figure 3.10 Contours of each core segment labelled with the number of pixels.

All individual contours are numbered and contain the total number of pixels included, which can serve as a guide for the calculation of RQD. Each photograph provided by Kore Geosystems captures 1m of core which is 10 times the size of a 10cm fragment. Assuming that the length of each fragment is proportional to its area (i.e., the width is relatively constant), and the core box has been mostly cropped from the image, the RQD can be estimated by the following equation:

$$RQD \approx \frac{\sum(\text{area of core fragments occupying more than 10\% of core box})}{\text{total area of core fragments}} \times 100\% \quad (3.1)$$

3.6 Deployment

The machine learning workflow is deployed as a web application using the streamlit package [34]. A web interface allows users to upload core images and view dynamically displayed prediction results. As a result, even non-programmers can easily access the tool and examine its performance without having to set up proper packages and environments. The prediction results (masks and RQD values) can also be saved locally for future analysis.

Chapter 4

Results

4.1 Experimental Results

The accuracy function for our prediction is defined by turning all outputted values into a matrix of digits for the segmentation mask. From there, their argmax is matched to the target's mask for each pixel, and an average is taken [35].

As shown in Figure 4.1 the training loss, validation loss, training time, and accuracy scoare are listed for the first 10 epochs. The final accuracy is 97.9% for our small dataset.

epoch	train_loss	valid_loss	acc_rock	time
0	0.838214	0.985264	0.923088	00:13
1	0.865667	0.838865	0.930969	00:13
2	0.760059	0.547633	0.945462	00:13
3	0.626819	0.299352	0.959107	00:13
4	0.528071	0.158674	0.965807	00:13
5	0.436023	0.133034	0.972528	00:13
6	0.374948	0.116781	0.971070	00:13
7	0.322914	0.117525	0.978148	00:13
8	0.297564	0.132753	0.963817	00:13
9	0.276449	0.110778	0.978786	00:13

Figure 4.1 Training loss, validation loss, and accuracy.

Figure 4.2 provides a visual illustration of how the model performance improved during

transfer learning (recall that transfer learning is used to train the model on smaller-sized images first). Figure 4.2a shows the predicted mask at half the original image's size, with a learning rate of 1e-3 found previously using the LR finder. Here, we can observe that the model often incorrectly labels white strips across the core sample as cracks. Figure 4.2b shows the prediction for the same downsized image, but with the LR decreased by 4 times. The model is better at segmenting intact core with stripped patterns, but there is still some confusion on the right end of the image. Figure 4.2c shows the final prediction for the full-size image and is the most accurate.

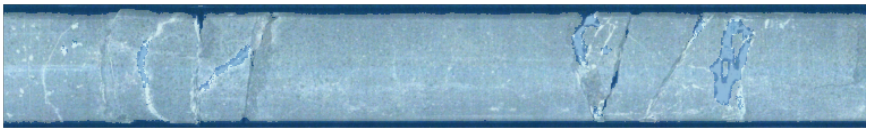

(a) Predicted mask with down-sized image, lr=1e-3

(b) Predicted mask with downsized image, lr=2.5e-4

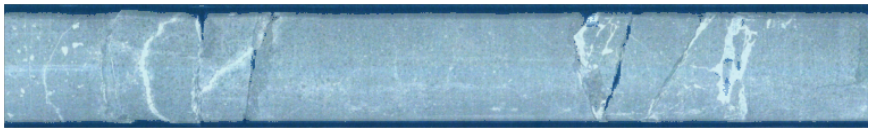

(c) Predicted mask with full image

Figure 4.2 Transfer learning using downsized images and higher learning rates.

Figure 4.3 to Figure 4.6 below are some sample prediction results generated by the ML workflow.

(a) Original Image

(b) Predicted mask

(c) Eroded mask

(d) Boundaries and enclosed area

Figure 4.3 Sample Prediction Results

(a) Original Image

(b) Predicted mask

(c) Eroded mask

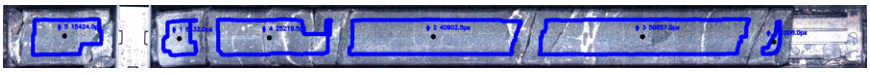

(d) Boundaries and enclosed area

Figure 4.4 Sample Prediction Results

(a) Original Image

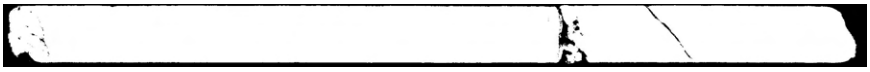

(b) Predicted mask

(c) Eroded mask

(d) Boundaries and enclosed area

Figure 4.5 Sample Prediction Results

(a) Original Image

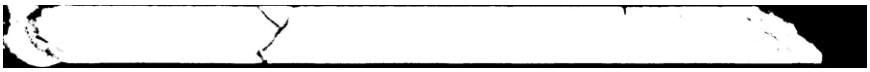

(b) Predicted mask

(c) Eroded mask

(d) Boundaries and enclosed area

Figure 4.6 Sample Prediction Results

RQD Prediction Results			
Sample Name	Predicted RQD	Actual RQD	% Difference
box6-Dry-row4	90.2%	86.7%	3.5%
box7-Dry-row1	86.9%	51.7%	35.2%
box7-Dry-row4	65.2%	90.0%	3.4%
box8-Dry-row3	93.4%	94.0%	-9.3%
box9-Dry-row2	84.7%	100.0%	-13.9%
box11-Dry-row3	86.1%	83.3%	9.2%
box12-Dry-row2	92.5%	90.0%	5.2%
box12-Dry-row4	95.2%	96.7%	2.0%
box17-Dry-row4	98.7%	100.0%	0%
box19-Dry-row3	70.9%	84.0%	13.1%

Table 4.1 RQD Prediction Results for the NDIBK01 dataset.

Table 4.1 shows the estimated RQD values against ground truth values, which are human-generated labels provided by Kore Geosystems. It can be observed that most predictions are within 10% of actual values which is mostly acceptable. In addition, while small prediction errors are mostly a result of the estimation method and the effect of erosion, much larger prediction errors are produced when two nearby core pieces are incorrectly identified as one intact rock as in the case of sample box7-Dry-row1.

4.2 Web Interface

A web interface was implemented which allows users to upload core images and view dynamically displayed prediction results. Figure 4.7 shows the initial interface where users can select a local image to upload. Figure 4.8 shows the uploaded image and the option to begin prediction. Figure 4.9 shows the predicted segmentation masks and the estimated RQD based on the area of individual core pieces. Automating and deploying the machine learning workflow as a web application allows non-developers to easily access the tool and examine its performance.

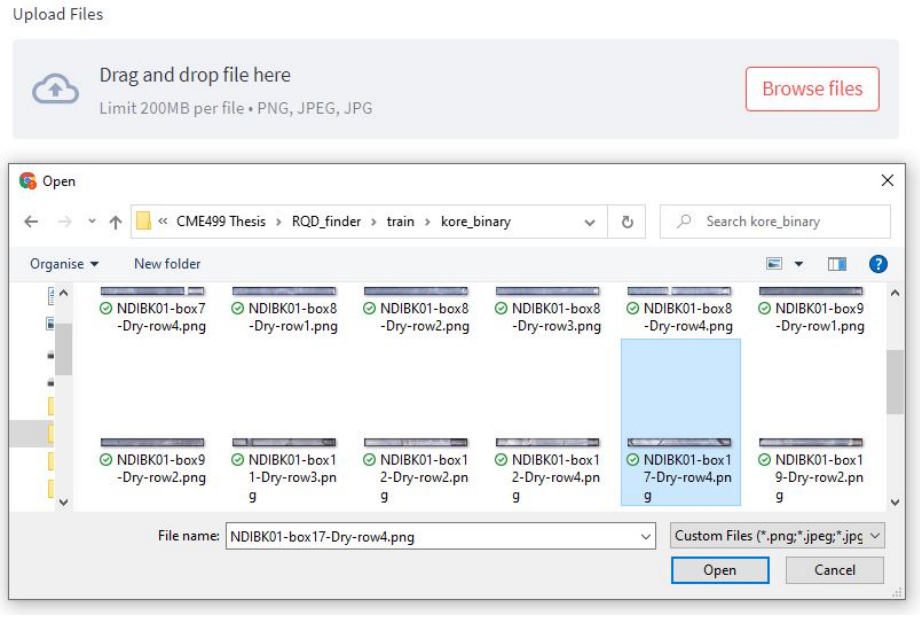

Figure 4.7 Initial interface for selecting local image.

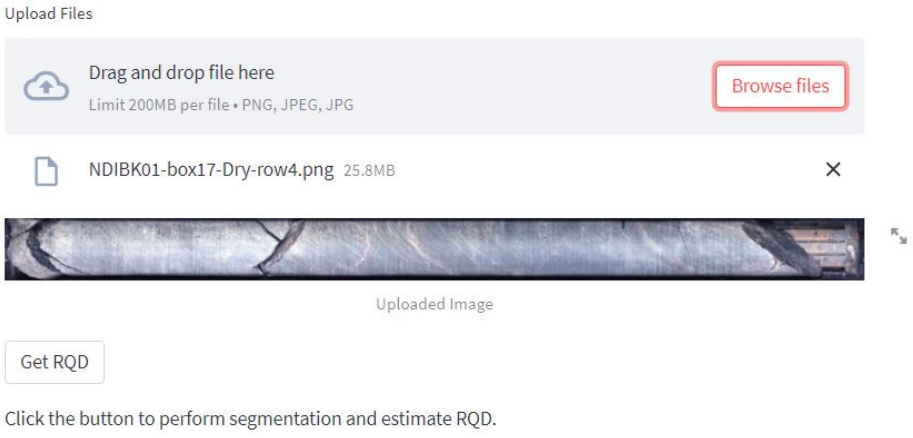

Figure 4.8 Interface showing uploaded image.

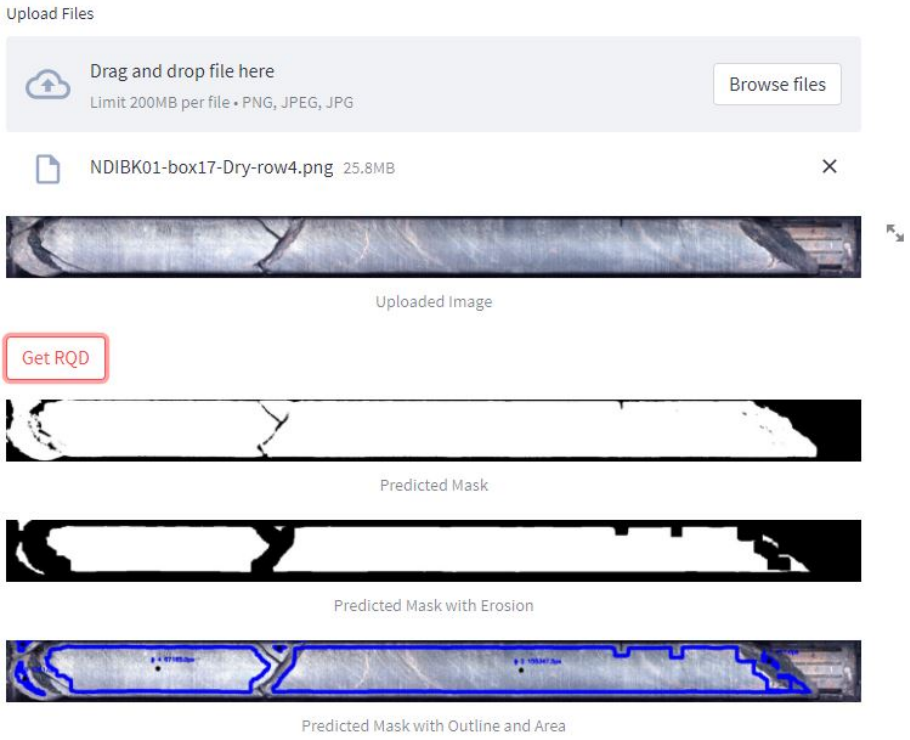

Figure 4.9 Interface showing prediction results.

Chapter 5

Discussion

5.1 Discussion of Results

In general, semantic segmentation using U-Net appears to be an effective method for RQD extraction in this small dataset. Although the number of training images is relatively low, making use of strategies such as image transformation and transfer learning can improve the performance and generalizability of the ML model. In addition, when carefully tuned, post-processing strategies such as erosion and dilation can help with the separation of close-by regions.

A few areas of improvement have been observed in the process of researching and developing the ML workflow. First of all, since the area without core (i.e., background) is significantly smaller than the core area, the accuracy results may be skewed. A more suitable loss function needs to be employed to properly capture the model performance during training. In addition, the model is sensitive to the appearance of rock and whether there are color patterns that resemble cracks. The model may not be able to generalize to another rock type that looks significantly different from the training images. Furthermore, a certain degree of down-sampling was required due to the RAM limitation in Colab. Since some of the cracks are very thin, not making use of the original high-definition photographs can compromise the model's capability to learn more subtle details.

The quality of the prediction is sensitive to the degree of erosion (i.e., the number of iterations for which the erosion kernel is applied). When there are not enough iterations, core pieces that are too close to each other can be merged into one piece, which results in an estimated RQD that is greater than the actual value. On the other hand, when there are too many iterations, core pieces that are too close to each other can be merged into one piece, which results in an estimated RQD that is greater than the actual value. In addition, dilation kernels have been observed to be unsuitable for many cases. Although dilation helps with smoothing out gaps in the predicted masks, it applying it universally to the entire image can

cause two separate regions to merge into one piece. As a result, smoothing and gap-filling is performed at the end using the watershed algorithm.

Another observation made while examining the predicted masks is that the learner is better at recognizing local than global characteristics. For example, although physical cracks usually extend across the entire width of the core, sometimes only part of the crack that is more visible can be recognized by the learner. In this case, erosion alone is not enough to separate these pieces as shown in Figure 5.1. One possible solution is to implement operators that only erode in the vertical direction. However, this method mainly works for straight, perpendicular cracks and may be less effective for angled cracks.

In terms of the predicted RQD values, it should be noted that the predictions are estimations only because the algorithm is based on area, not length. If the width of the core pieces are not consistent or do not match the width of the core box, or if the core box is not cropped out of the image, the area-based prediction can be less accurate. In addition, when two nearby core pieces are not correctly separated and are predicted as one continuous piece, the error in the resulted RQD estimation can drastically increase.

(a) Original Image

(b) Predicted mask

(c) Eroded mask

(d) Boundaries and enclosed area

Figure 5.1 Sample prediction where only a portion of the crack is detected

Chapter 6

Conclusion

The main conclusions from this thesis project are summarized as follows:

1. Machine Learning has promising applications for various core logging processes.
2. Semantic segmentation using U-Net appears to be a viable method for segmenting intact rock from core boxes.
3. Transfer learning strategies (e.g., training the model on ImageNet and training the model on downsized images first) can be applied to reduce train time improve the overall accuracy.
4. Morphological transformations such as dilation and erosion can be used in the post-processing step to improve the quality of predicted masks.
5. Additional tools such as the watershed and contour-finding algorithm can be applied to calculate the area of individual core segments which can be translated into an RQD index.
6. The ML workflow can be automated and deployed as a web application to improve usability by facilitating ease-of-access and dynamically displaying the results.

Chapter 7

Recommendation

7.1 Challenges

Despite the potential of machine intelligence and some promising results, many challenges still need to be overcome for successful application in the mining industry [1]. One challenge that is present for many machine learning tasks in general is the availability of data. Machine learning models require large datasets with high quality labels, which are often not available or difficult to acquire. These models also require the input to be clean, well-organized and in a truly digital format, which is not the case with a lot of the data collected in mineral exploration today. Significant improvements are needed in the way data is collected, organized and stored before the application of machine learning becomes viable.

Furthermore, machine learning methods must be well-adapted to geoscience problems, which generally involve complex time and spatial relationships between variables. Strong domain expertise is required to understand which data is necessary to solve a problem, how the data should be processed, and predictions can be interpreted. In addition, ML is a complex field with different algorithms adapted to different problems. Many ML algorithms are based on patterns within the provided data, rather than reflecting the underlying cause of the observed relationships (i.e., they are empirical). This makes predictions based on machine learning tools susceptible to errors in the absence of model validation by domain experts, because it is easy to introduce bias to the model if either the input data or the problem is misunderstood. For these reasons, machine learning should be used as a tool to help geoscientists with decision-making and not to replace them completely. A multi-disciplinary team with both machine-learning and geoscience expertise is required to successfully implement a machine learning solution to the problem of core logging.

7.2 Future Work

To improve the prediction accuracy, more images should be annotated and used in the training process. More careful tuning of hyper-parameters and the U-net architecture can be helpful to fit a model to this specific problem. In addition, the post-processing step can be improved to more accurately translate the number of pixels within each contour to an RQD measurement. Furthermore, other image segmentation algorithms such as Mask-RCNN as well as unsupervised methods such as clustering can be explored and compared with the U-Net approach. The web application can also be refined to improve usability and scalability.

The mining industry is seeing an increasing number of modern solutions for drill-core logging using machine learning algorithms. Machine learning models are extremely effective for problems that involve repetitive tasks and a large amount of multivariate, high-quality, and well-labeled data. However, training and implementing a machine learning model for core logging requires strong domain expertise in geoscience. The automated logs must be qualitatively assessed and verified by experienced mine geologists prior to further processing of the data, such as refinement of geological models. To stay at the forefront of their field and to add value to the mining industry, the new generation of geologists can work with machine learning engineers to develop and utilize these tools and allow machine learning applications to reach their full potential.

7.3 Open-source Databases

To properly train and deploy machine learning models, access to large, high-quality datasets is essential. Below is a non-exhaustive list of online, open-source databases containing drill-core data for further development.

- National Virtual Core Library (NVCL): an Australia-wide drill-core database comprising high-resolution imagery and mineralogical data from hyperspectral scanning; the data is being collected using CSIRO's HyLogger-system and is available on the AuScope Discovery Portal and the AUSGIN Geoscience Portal
- National Drilling Initiative (NDI) portal: data collected from drilling campaigns including the East Tennant Campaign and the South Nicholson Campaign with detailed geological logs, portable XRF and Minalyze geochemical logs, Hylogger hyperspectral imagery, multi-tool wireline geophysical data, drill-core imagery, and rock chip imagery
- British borehole collection database: high-resolution colour images of continuous drill-core and core samples from onshore boreholes and offshore hydrocarbon wells;

details of thin sections are also available in the BRITROCKS mineralogy and petrology collections database

- Geoscience Collections of Estonia: 22,500 images of drill-core (boxes)
- National Offshore Petroleum Data and Core Repository: samples of geoscience material and digital data such as well logs and core photography provided by Geoscience Australia
- Geological Survey of Sweden (SGU): hyperspectral and high-resolution optical RGB images of 200,000 meters of drill-core

References

[1] A. Caté, Machine learning and artificial intelligence, Technical Report, srk consulting, 2019.

[2] A. Caté, L. Perozzi, E. Gloaguen, M. Blouin, Machine learning as a tool for geologists, Leading Edge 36 (2017) 215–219. doi:10.1190/tle36030215.1.

[3] L. Webb, The future of mining and mining geology - advances in technology, AI and automation. — Datarock, 2019. URL: https://www.datarock.com.au/news/the-future-of-mining-and-mining-geology-advances-in-technology-ai-and-automation.

[4] A. Lateef, Most used rock mass classifications for underground opening (2010).

[5] O. Ronneberger, P. Fischer, T. Brox, U-net: Convolutional networks for biomedical image segmentation, CoRR abs/1505.04597 (2015). URL: http://arxiv.org/abs/1505.04597. arXiv:1505.04597.

[6] Hyperspectral Mineralogy & Deep Learning | Life Cycle Geo, ???? URL: https://www.lifecyclegeo.com/hyperspectral-mineralogy-deep-learning/.

[7] K. He, X. Zhang, S. Ren, J. Sun, Deep residual learning for image recognition (2015). arXiv:1512.03385.

[8] S. M. Gandhi, B. C. Sarkar, Essentials of Mineral Exploration and Evaluation - 1st Edition, Elsevier, 2016. URL: https://www.elsevier.com/books/essentials-of-mineral-exploration-and-evaluation/gandhi/978-0-12-805329-4.

[9] I. C. C. Acosta, M. Khodadadzadeh, R. Tolosana-Delgado, R. Gloaguen, Drill-core hyperspectral and geochemical data integration in a superpixel-based machine learning framework, IEEE Journal of Selected Topics in Applied Earth Observations and Remote Sensing 13 (2020) 4214–4228. doi:10.1109/JSTARS.2020.3011221.

[10] E. Littlefield, W. Calvin, P. Stelling, T. Kent, Reflectance spectroscopy as a drill core logging technique: An example using core from the Akutan, in: Transactions - Geothermal Resources Council, volume 36, 2012, pp. 1283–1291.

[11] M. Blouin, A. Caté, L. Perozzi, E. Gloaguen, Automated facies prediction in drillholes using machine learning, 79th EAGE Conference and Exhibition 2017 - Workshops (2017). doi:10.3997/2214-4609.201701657.

[12] P. S. Ross, A. Bourke, B. Fresia, A multi-sensor logger for rock cores: Methodology and preliminary results from the Matagami mining camp, Canada, Ore Geology Reviews 53 (2013) 93–111. doi:10.1016/j.oregeorev.2013.01.002.

[13] M. Klawitter, R. Valenta, Automated Geological Drill Core Logging Based on XRF Data

Using Unsupervised Machine Learning Methods, 6th International Conference on Geology and Mine Planning (2019) 1–8.

[14] E. J. Hill, M. A. Pearce, J. M. Stromberg, Improving Automated Geological Logging of Drill Holes by Incorporating Multiscale Spatial Methods, Mathematical Geosciences 53 (2021) 21–53. doi:10.1007/s11004-020-09859-0.

[15] N. Schnitzler, P. S. Ross, E. Gloaguen, Using machine learning to estimate a key missing geochemical variable in mining exploration: Application of the Random Forest algorithm to multi-sensor core logging data, Journal of Geochemical Exploration 205 (2019) 106344. URL: https://doi.org/10.1016/j.gexplo.2019.106344. doi:10.1016/j.gexplo.2019.106344.

[16] S. Chen, K. Hattori, E. C. Grunsky, Identification of sandstones above blind uranium deposits using multivariate statistical assessment of compositional data, Athabasca Basin, Canada, Journal of Geochemical Exploration 188 (2018) 229–239. doi:10.1016/j.gexplo.2018.01.026.

[17] F. van der Meer, Analysis of spectral absorption features in hyperspectral imagery, International Journal of Applied Earth Observation and Geoinformation 5 (2004) 55–68. URL: https://research.utwente.nl/en/publications/analysis-of-spectral-absorption-features-in-hyperspectral-imagery. doi:10.1016/j.jag.2003.09.001.

[18] D. Wang, R. Lagerstrom, C. Sun, C. Laukamp, M. Quigley, L. Whitbourn, P. Mason, P. Connor, L. Fisher, Automated vein detection for drill core analysis by fusion of hyperspectral and visible image data, M2VIP 2016 - Proceedings of 23rd International Conference on Mechatronics and Machine Vision in Practice (2017) 1–6. doi:10.1109/M2VIP.2016.7827317.

[19] I. C. C. Acosta, M. Khodadadzadeh, L. Tusa, P. Ghamisi, R. Gloaguen, A Machine learning framework for drill-core mineral mapping using hyperspectral and high-resolution mineralogical data fusion, IEEE Journal of Selected Topics in Applied Earth Observations and Remote Sensing 12 (2019) 4829–4842. doi:10.1109/JSTARS.2019.2924292.

[20] L. Tuşa, M. Khodadadzadeh, C. Contreras, K. R. Shahi, M. Fuchs, R. Gloaguen, J. Gutzmer, Drill-core mineral abundance estimation using hyperspectral and high-resolution mineralogical data, Remote Sensing 12 (2020). doi:10.3390/rs12071218.

[21] I. C. Contreras, M. Khodadadzadeh, R. Gloaguen, H.-Z. Dresden-Rossendorf, MULTI-LABEL CLASSIFICATION FOR DRILL-CORE HYPERSPECTRAL MINERAL MAPPING (2020). URL: https://doi.org/10.5194/isprs-archives-XLIII-B3-2020-383-2020. doi:10.5194/isprs-archives-XLIII-B3-2020-383-2020.

[22] M. Blouin, Automated drillcore description based on core images and machine learning, Technical Report, PDAC 2018 Convention, 2018.

[23] M. M. MEZGHANI, S. H. SHAMMARI, F. A. ANIFOWOSE, AUTOMATED CORE DESCRIPTION, 2017.

[24] A. V. Ivchenko, E. E. Baraboshkin, L. S. Ismailova, D. M. Orlov, D. A. Koroteev, E. Y. Baraboshkin, Core Photo Lithological Interpretation Based on Computer Analyses, in: 20th International Sedimentological Congress, 2, Quebec, 2018.

[25] E. E. Baraboshkin, L. S. Ismailova, D. M. Orlov, E. A. Zhukovskaya, G. A. Kalmykov, O. V.

Khotylev, E. Y. Baraboshkin, D. A. Koroteev, Deep convolutions for in-depth automated rock typing, Computers and Geosciences 135 (2020) 1–24. doi:10.1016/j.cageo.2019.104330.

[26] D. Gleeson, Datarock machine learning drill core analysis tool hits major milestone - International Mining, 2020. URL: https://im-mining.com/2020/06/10/datarock-machine-learning-drill-core-analysis-tool-hits-major-milestone/.

[27] D. D.U., D. D.W., Rock Classification Systems for Engineering Purposes, American Society for Testing and Materials, 1988.

[28] BGS, British Geological Survey, 2022. URL: https://www.bgs.ac.uk/.

[29] Kore Geosystems, Kore Geosystems, 2022. URL: https://www.koregeosystems.com/.

[30] MIT CSAIL, LabelMe, 2022. URL: https://github.com/wkentaro/labelme.

[31] Google, Colab Pro, 2022. URL: https://colab.research.google.com/signup.

[32] OpenCV, Image Processing Module, 2022. URL: https://docs.opencv.org/3.4/d7/dbd/group__imgproc.html.

[33] J. Deng, W. Dong, R. Socher, L.-J. Li, K. Li, L. Fei-Fei, ImageNet: A Large-Scale Hierarchical Image Database, in: CVPR09, 2009.

[34] streamlit, Streamlit, 2022. URL: https://streamlit.io/.

[35] fastai, Walk with fastai, 2022. URL: https://walkwithfastai.com/Segmentation.